Multilateral Closed-Loop Geothermal Systems as a Zero-Emission Load-Following Resource

Michael Holmes[(1)], Matthew Toews[(1)], Jesse Jenkins[(2)], and Nestor Sepulveda[(2)]

[(1)] Eavor Technologies Inc.
[(2)] DeSolve, LLC

Keywords

Geothermal, closed-loop, multilateral, net-zero, load-following, thermodynamics, zero-emission, modelling, renewable, green energy, Eavor-Loop, Eavor-Lite

ABSTRACT

The Eavor-Loop™, a multilateral closed-loop geothermal system (MCLGS), is introduced as a zero-emission load-following resource (ZELFR) that is globally scalable and can provide baseload or dispatchable electricity. For any electrical grid to reach net-zero, ZELFR or large-scale energy storage is required to balance intermittent renewables like solar and wind and provide grid stability. Given the declining costs of intermittent renewables and their increased utilization in modern grids, the ability to load follow is both crucial and highly valued.

The objectives of this paper are two-fold. First, we prove the technical feasibility of MCLGS to provide flexible power using first principles-based models. Second, we demonstrate the value enhancement of flexible operation with a case study of the United States Western Interconnection power transmission grid using an electricity resource capacity expansion model.

A transient, fully coupled wellbore + thermal model was developed and validated using over a year of operating data from the Eavor-Lite™ facility, a full-scale Eavor-Loop™ demonstration project in Alberta, Canada. Recent modelling work, coupled with field trials, has proven the feasibility of Eavor-Loop™ to provide flexible energy for load-balancing or peak-matching with a minimal impact on lifetime energy extraction. Transient operation allows the system to recharge during low demand periods.

To demonstrate the value of Eavor-Loop™ in a net-zero grid, an electricity resource capacity expansion model (GenX) was used. GenX is a constrained optimization model that determines the mix of electricity generation and storage required to meet electricity demand while minimizing system cost. Flexible Eavor-Loop™ operation provides stability for the grid, matching electricity generation with demand, and reduces annual total system cost by up to $20B (21%) in a base case and up to $403B (81%) in an extreme case. Inclusion of Eavor-Loop™ also reduces land use required by up to 49%, saving 25 acres in a base case and 48 acres in an extreme case for each megawatt of Eavor-Loop™ installed.

1. Introduction

Governments and corporations around the world are facing increased pressure to reduce their greenhouse gas (GHG) emissions and create plans to transition their energy use away from fossil fuels. Energy is vital to quality of life, and this theme has been highlighted throughout the COVID-19 pandemic as well as events like the Texas power crisis of February 2021. Transitioning away from fossil fuels will not be easy: in 2019, 84% of primary energy use was provided by a combination of oil, gas, and coal (bp, 2020). Clearly, we have a long way to go.

Several prominent research institutions have analyzed pathways to net-zero, with 2050 being a common timeline for achieving this goal. The European Commission estimates that the share of electricity in final energy consumption will grow from 23% today towards 50% in 2050, with a majority of the growth coming from renewable energy (European Commission, 2020). The International Energy Agency (IEA) recently released a roadmap to net-zero, concluding that almost half of the global reductions in CO_2 emissions in 2050 will come from technologies currently at the demonstration or prototype phase, with one of the biggest innovation opportunities being energy storage (International Energy Agency, 2021). Factoring in increased total energy demand from a growing global population and improved energy access in developing countries makes the task even more daunting.

As penetration of intermittent renewables such as solar and wind increases, two challenges emerge: physical space constraints and concerns regarding grid stability and resiliency. Many countries are constrained on land area and cannot designate a substantial portion of their land to be covered with solar panels or wind turbines, especially when this land is required for food production to support a growing population. To transition to net-zero, these countries will require a zero-emission energy source with an energy density comparable to that of fossil fuels. Countries with a larger land mass can continue to build solar and wind capacity, but grid stability and resiliency become a concern as intermittent renewables make up a larger portion of electricity generation. People need energy, regardless of whether the sun is shining or the wind is blowing. Sepulveda et al. investigated the role of firm low-carbon resources in deep decarbonization and found that availability of firm low-carbon technologies, such as natural gas combined cycle (NGCC) equipped with carbon capture and storage (CCS), reduces electricity cost by up to 62% in fully decarbonized scenarios (Sepulveda, Jenkins, de Sisternes, & Lester, 2018). Although firm low-carbon technologies can deliver system value, they frequently face public opposition due to their environmental impacts, namely the fact that they are non-renewable.

Geothermal energy is clean and renewable and has been used for heat and electricity generation for over a century (Fallah, et al., 2021). However, the requirement of high geothermal gradients and a permeable aquifer has limited the scalability of geothermal energy, rendering it a niche technology suitable only in global hotspots (Rybach, 2010). Closed-loop geothermal systems (CLGS) offer a solution to the scalability issue. CLGS rely only on conductive heat transfer, removing the need for a permeable aquifer. CLGS also have no water use, no fracking, no induced seismicity, no corrosion/erosion/scaling, no fluid disposal, no requirement for rare earth metals, and a low environmental footprint (Toews, Riddell, Vany, & Schwarz, 2020). The primary drawback of CLGS is that they are limited by the rate of conductive heat transfer through rock, which is a slow physical process. The required wellbore area in contact with the hot rock is very large to overcome this limitation and make the overall project economical. Drilling multilateral

closed-loop geothermal systems (MCLGS), whereby a single vertical well is connected to multiple lateral wells for heat harvesting, is one way to create a sufficiently large contact area.

This paper introduces one such MCLGS, the Eavor-Loop™, as a globally scalable zero-emission resource capable of providing firm or load-following electricity (a zero-emission load-following resource, or ZELFR). The objectives of this paper are two-fold. First, we prove the technical feasibility of the Eavor-Loop™ to provide flexible power using first-principles based models validated by 16 months of operational data from an Eavor-Loop™ field demonstration in Alberta, Canada. Second, we demonstrate the system value of the Eavor-Loop™ in a net-zero grid with a case study of the United States Western Interconnection power transmission grid using an electricity resource capacity expansion model.

2. Eavor-Loop™ thermodynamic model

2.1 Model formulation

The energy output of an Eavor-Loop™ system can be predicted using various engineering approaches to model the transient heat transfer from the surrounding rock to the fluid flowing through the wellbore. This paper introduces a method of numerical simulation of the transient, 2-dimensional heat conduction in the rock surrounding the wellbore coupled with a numerical simulation of the transient 1-dimensional energy and momentum equations for fluid flow inside the wellbore.

Fourier's law of heat conduction and the conservation of energy equation can be combined to derive the partial differential equation (PDE) that governs the transient conduction of thermal energy in rock with a constant thermal conductivity:

$$\rho_r C_{p,r}\left(\frac{\partial T}{\partial t}+v_r\frac{\partial T}{\partial r}+\frac{v_\theta}{r}\frac{\partial T}{\partial \theta}+v_z\frac{\partial T}{\partial z}\right)=k_r\left(\frac{1}{r}\frac{\partial}{\partial r}\left(r\frac{\partial T}{\partial r}\right)+\frac{1}{r^2}\frac{\partial^2 T}{\partial \theta^2}+\frac{\partial^2 T}{\partial z^2}\right)+\dot{g} \quad (1)$$

where ρ_r is the rock density
$C_{p,r}$ is the rock heat capacity
T is the rock temperature
t is time
v is velocity
r is the radial direction
θ is the angular direction
z is the axial direction
k_r is the rock thermal conductivity
$\dot{g}$ is the rate of heat generation

Assuming transient heat transfer by conduction only, no thermal interaction between adjacent wellbores, and no angular variation in temperature yields:

$$v_r = v_\theta = v_z = 0$$
$$\frac{\partial T}{\partial \theta} = 0$$
$$\dot{g} = 0$$

Equation 1 reduces to:

$$\frac{1}{\alpha_r}\frac{\partial T}{\partial t} = \frac{1}{r}\frac{\partial}{\partial r}\left(r\frac{\partial T}{\partial r}\right) + \frac{\partial^2 T}{\partial z^2} \quad (2)$$

where α_r is the thermal diffusivity of the rock: $\alpha_r = \frac{k_r}{\rho_r C_{p,r}}$

The transient energy equation for the 1D fluid flow in the wellbore along the axial coordinate system can be expressed as:

$$\frac{\partial \rho_f e}{\partial t} + \frac{\partial G(h+gy)}{\partial z} = U\left(T_{rw} - T_f\right) \quad (3)$$

where ρ_f is the fluid density
e is the internal energy of the fluid
G is the mass flux of fluid flowing through the wellbore
h is the enthalpy of the fluid
g is the acceleration due to gravity
y is the position in the vertical direction (parallel to gravity)
U is the heat transfer coefficient from the rock/wellbore boundary to the fluid
T_{rw} is the temperature of the rock at the rock/wellbore boundary
T_f is the temperature of the bulk fluid in the wellbore

Note that the change in kinetic energy has been neglected in equation 3 as this contribution is negligible compared to the internal energy and enthalpy change of the fluid. In addition, the conservation of mass has been invoked for an incompressible fluid so the mass flux, G, is constant along the length of the wellbore. The heat transfer coefficient U is comprised of any conductive resistance between the rock and the wellbore (i.e., casing and cement in the vertical sections) and convective resistance of the flowing fluid.

A quasi-steady state version of the momentum equation is employed whereby the pressure drop of the fluid is calculated using Colebrook White type correlation. Given the simplicity of the momentum equation, it is not repeated here.

2.2 Initial and boundary conditions

The temperature field of the rock and fluid at time t=0 must be specified along with boundary conditions for the temperature, pressure, and flowrate of the fluid at the inlet of the loop. The rock boundary temperature and radius must also be specified. For all simulations, the boundary rock radius is set large enough such that it has not been impacted by the thermal front and the boundary temperature remains at virgin rock temperature. At the boundary between the rock and the fluid flowing through the loop, the heat flux must be continuous such that the heat flux calculated using Fourier's Law is equivalent to the heat flux entering the wellbore and being transferred to the fluid:

$$k_r\frac{\partial T}{\partial r} = U\left(T_{rw} - T_f\right) \quad (4)$$

2.3 Discretization and numerical solution

The PDE describing the transient 2D conduction in the rock can be solved numerically by integrating equation 2 over a discrete finite control volume, $dV = 2\pi r\, dr\, dz$ and specified time step Δt:

$$\frac{1}{\alpha_r}\pi\left(r_{i+1}^2 - r_i^2\right)\left(z_{j+1} - z_j\right)\frac{T_{i,j}^{n+1} - T_{i,j}^{n}}{\Delta t} = 4\pi\left(z_{j+1} - z_j\right)\left(r_{i+1}\frac{T_{i+1,j}^{n+1} - T_{i,j}^{n+1}}{r_{i+2} - r_i} - r_i\frac{T_{i,j}^{n+1} - T_{i-1,j}^{n+1}}{r_{i+1} - r_{i-1}}\right)$$
$$+\ 2\pi\left(r_{i+1}^2 - r_i^2\right)\left(\frac{T_{i,j+1}^{n} - T_{i,j}^{n}}{z_{j+2} - z_j} - \frac{T_{i,j}^{n} - T_{i,j-1}^{n}}{z_{j+1} - z_{j-1}}\right) \quad (5)$$

where i indexes the radial direction, j indexes the axial direction, and n indexes time.

Note that the radial derivatives on the right-hand side of equation 5 are implicitly calculated at the new time step (n+1) whereas the axial derivatives are explicitly calculated at the previous time step (n). This is acceptable as the spacing in the axial direction is much larger than the radial direction. Consequently, the stability criterion in the explicit numerical treatment in the axial direction is not violated.

The transient 1D energy equation (equation 3) for the wellbore flow is discretized in the following manner:

$$\rho_f \pi r_w^2 \Delta z \frac{\left(\hat{h}_{0,j}^{n+1} - \hat{h}_{0,j}^{n}\right)}{\Delta t} + G\pi r_w^2\left(\left(\hat{h}_j^{n+1} - \hat{h}_{j-1}^{n+1}\right) + g\Delta y\right) = U_j 2\pi r_w \Delta z\left(T_{1,j}^{n+1} - T_{0,j}^{n}\right) \quad (6)$$

Equation 6 makes use of the specific enthalpy ($\hat{h}$) in place of heat capacity and temperature to properly model the Joule-Thomson effect, which has a large impact on the temperature change of the fluid in the vertical sections of the loop.

Linear, least-squared regression correlations were derived for working fluid thermophysical properties (enthalpy, density, viscosity, and thermal conductivity) obtained from NIST Refprop (National Institute of Standards and Technology, 2020). Thermophysical properties are calculated based on the inlet conditions of each wellbore grid block for each time step. The axial grid spacing is maintained sufficiently small to ensure that temperature and pressure changes between grid blocks are minimal, maintaining validity of the assumption of constant thermophysical properties within each grid block.

The resulting system of algebraic equations for all the control volumes for the rock and wellbore fluid along with specified boundary conditions are solved using the Tri-Diagonal Matrix Algorithm to compute the temperature field at the new time step, $T_{i,j}^{n+1}$ based on the previous time step $T_{i,j}^{n}$.

2.4 Field validation of transient model

2.4.1 Eavor-Lite™ overview

The Eavor-Loop™ Demonstration Project ("Eavor-Lite™") is a full-scale prototype of a multilateral closed-loop geothermal system intended to derisk the key technical components, including thermodynamic validation, and serve as a research facility for future technology commercialization. The multilateral closed-loop system, shown in Figure 1 below, consists of a large U-shaped well drilled to 2.4 km depth, two parallel laterals, each of 1700m length, and a pipeline connecting the two sites on surface. A water-based working fluid circulates in the inlet well (B→C), through the parallel horizontal wellbores (C→D) where the working fluid receives heat from the rock via conduction, and rises up the outlet well (D→E) at an elevated temperature. The density difference between the inlet and outlet well creates a thermosiphon which is sufficient to overcome hydraulic losses, eliminating the need for a circulating pump. A test facility on the

surface measures all relevant performance data and cools the working fluid for re-circulation in the pipeline (A→B) and back to the inlet well.

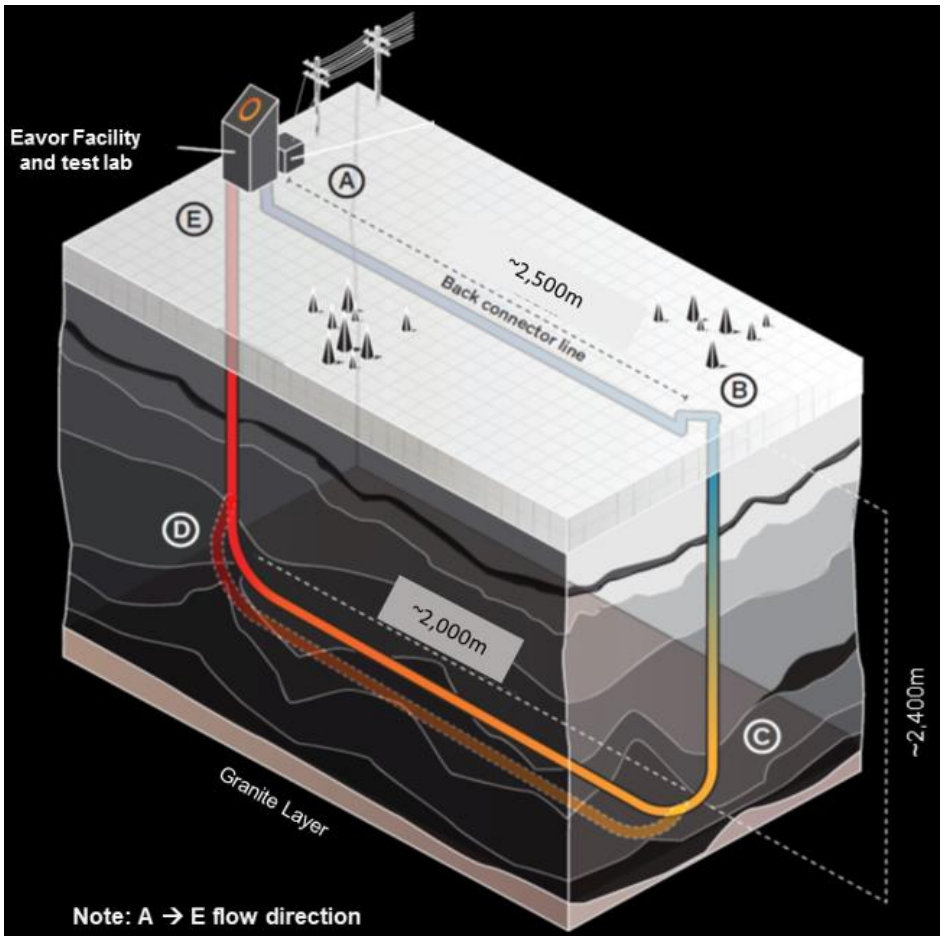

Figure 1: Eavor-Lite™ overview

2.4.2 Prediction of Eavor-Lite™ performance

The transient 2D model introduced in section 2.1 was used to predict the measured performance data from Eavor-Lite™. The model was history matched using 60 days of time series production data comprising outlet wellhead temperature, outlet wellhead pressure, and flowing temperature at various depths measured by a 6-point thermocouple in the outlet well. Time series of measured circulation rate, inlet wellhead temperature, and inlet wellhead pressure were provided as inputs. History match parameters were the vertical and lateral rock thermal conductivities. The history match was performed using a genetic algorithm to minimize an objective function specified as a weighted sum of squared error terms between the model's prediction and the measured data. Rock thermal conductivities, and accordingly thermal performance of the system, were calculated to be within 5% of the values estimated prior to drilling the loop, highlighting the predictability of the Eavor-Loop™ system.

Figure 2 below shows the measured and predicted outlet temperature. The vertical line separates the data used for the history match (left) from the extrapolation and prediction (right). Circulation rate is shown for reference. Note that periods where there is no measured wellhead temperature correspond to periods where the loop was shut down (circulation rate of 0) for thermal recharge testing. To date, the model has been used to successfully predict over 16 months of operating data with a mean absolute error of only 0.19°C (0.37%).

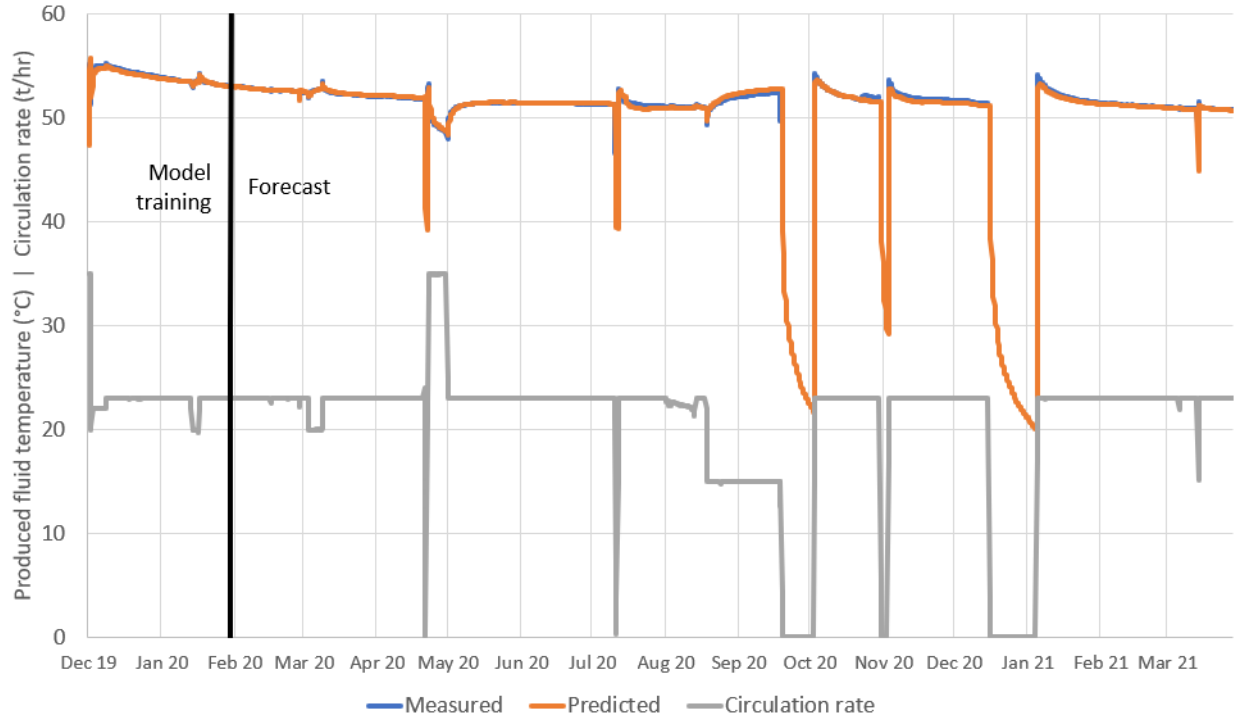

Figure 2: Measured and simulated outlet wellhead temperature for the Eavor-Lite™ demonstration project

Several trials have been run to prove the ability of the Eavor-Loop™ to operate in a flexible fashion. The focus of this paper will be on the first trial, run from September 22 to October 6, 2020. During this trial, circulation was stopped completely for 14 days to validate the thermal recharge predicted by the model, a critical requirement for proving flexible operation. The predicted and measured temperatures in the outlet wellbore thermocouple string are shown in Figure 3. Closer to the surface, where the virgin rock temperature is cooler, a larger reduction in stagnant wellbore temperature is observed both in the field data and the model. The rate of heat dissipation is governed by the thermal drawdown during circulation prior to the shut in as well as the thermal diffusivity of the surrounding rock. The ability of the model to accurately predict the observed temperature drawdown in the vertical well gives confidence that all the relevant physics are captured and the calculated thermal conductivities are correct.

Figure 3: Measured and predicted temperature falloff in the outlet well thermocouple during the thermal recharge test

Figure 4 and Figure 5 show the predicted temperature profile along the lateral wellbore on September 21, 2020 (immediately prior to the recharge trial) and October 4, 2020 (at the end of the recharge trial prior to commencing circulation), respectively. Figure 6 and Figure 7 show how the radial rock temperature at the heel and toe, respectively, change during and after the trial. The thermal recharge of the rock is evident, most notably at the heel of the well where the near-wellbore temperature increased from 36°C during circulation to 64°C after 14 days of recharge. This is intuitive given the fluid temperature is lowest, and therefore the heat flux is the highest, at the heel.

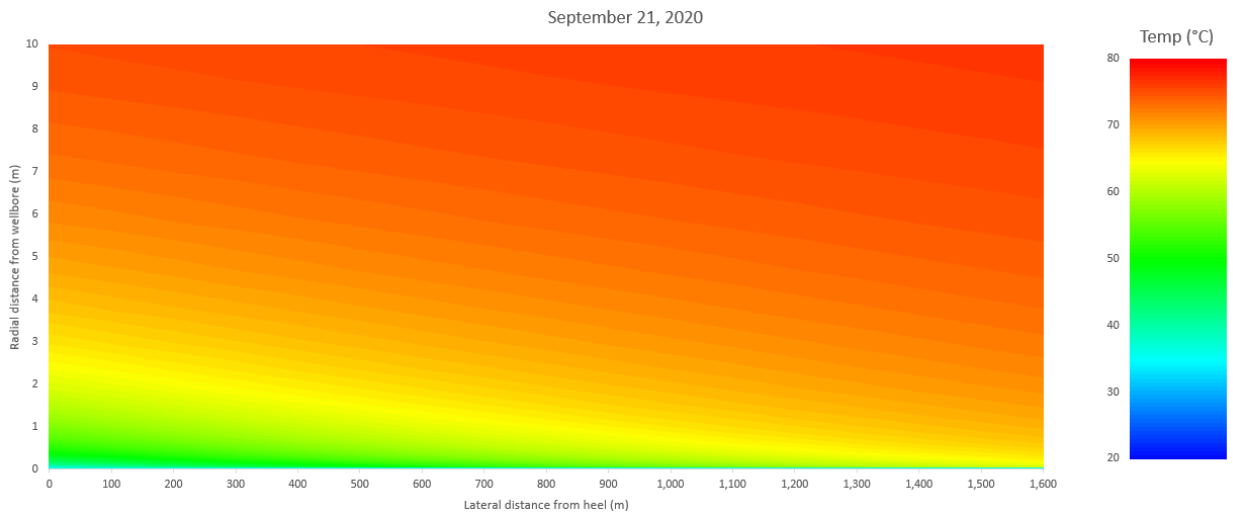

Figure 4: Simulated temperature profile along the lateral wellbore immediately prior to thermal recharge trial

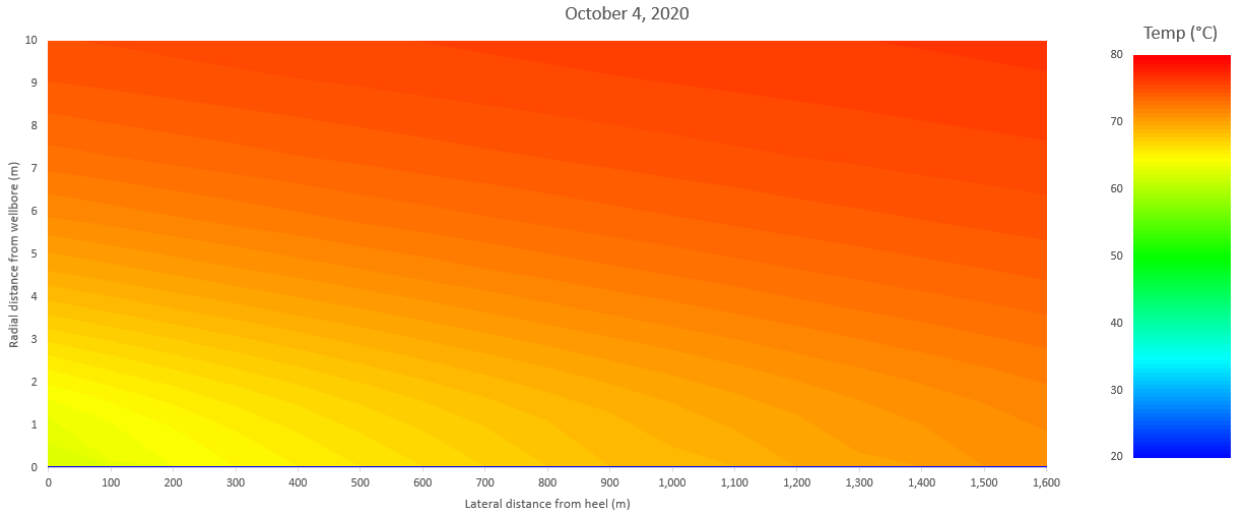

Figure 5: Simulated temperature profile along the lateral wellbore at the end of the recharge trial prior to commencing circulation

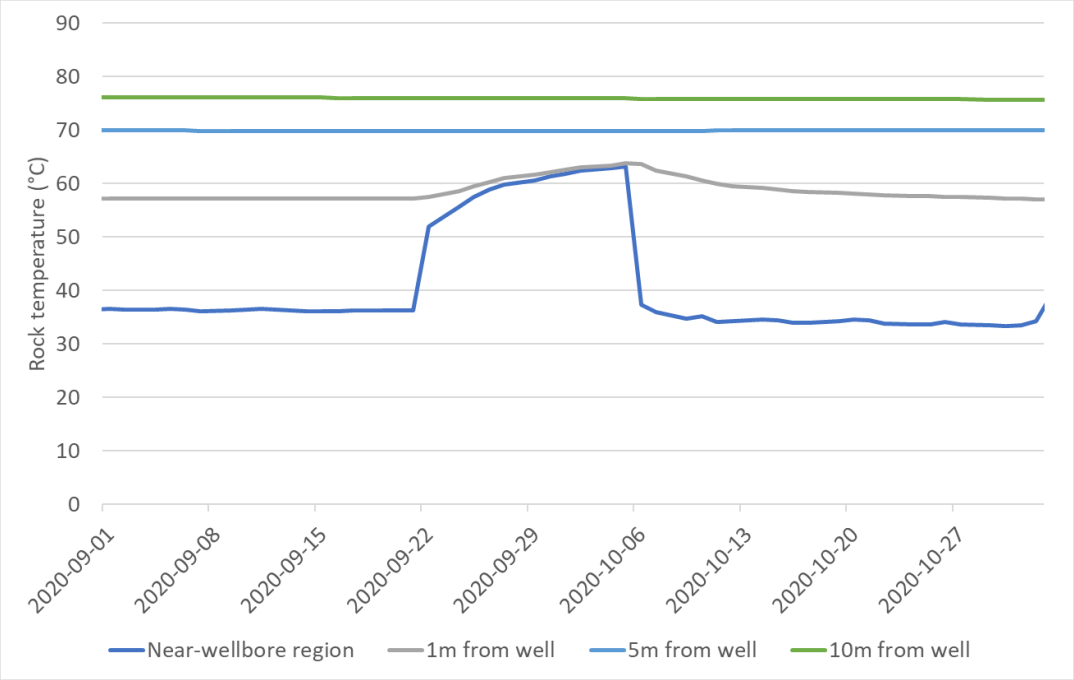

Figure 6: Radial rock temperature profiles at the heel of the well showing thermal recharge of the near-wellbore region

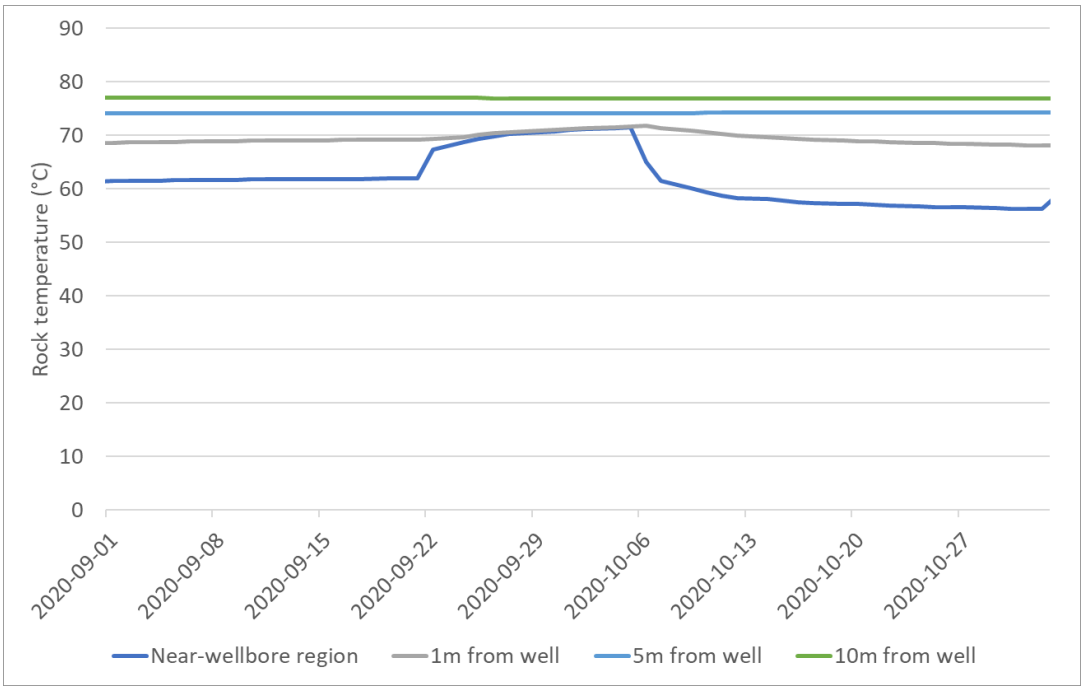

Figure 7: Radial rock temperature profiles at the toe of the well showing thermal recharge of the near-wellbore region

2.5 Extrapolation to future projects

The same physics outlined in this paper, built into Eavor's transient model, and validated with Eavor-Lite™ can be used to estimate the performance of future Eavor-Loop™ projects. To be truly scalable with a low levelized cost of electricity (LCOE), novel drilling technology is required to enable deeper Eavor-Loops™ in hotter and harder crystalline basement rock – "Eavor-Loop™ 2.0" as illustrated in Figure 8. Such a configuration will massively reduce the LCOE of the Eavor-Loop™ system, enabling widespread adoption at gigawatt scale.

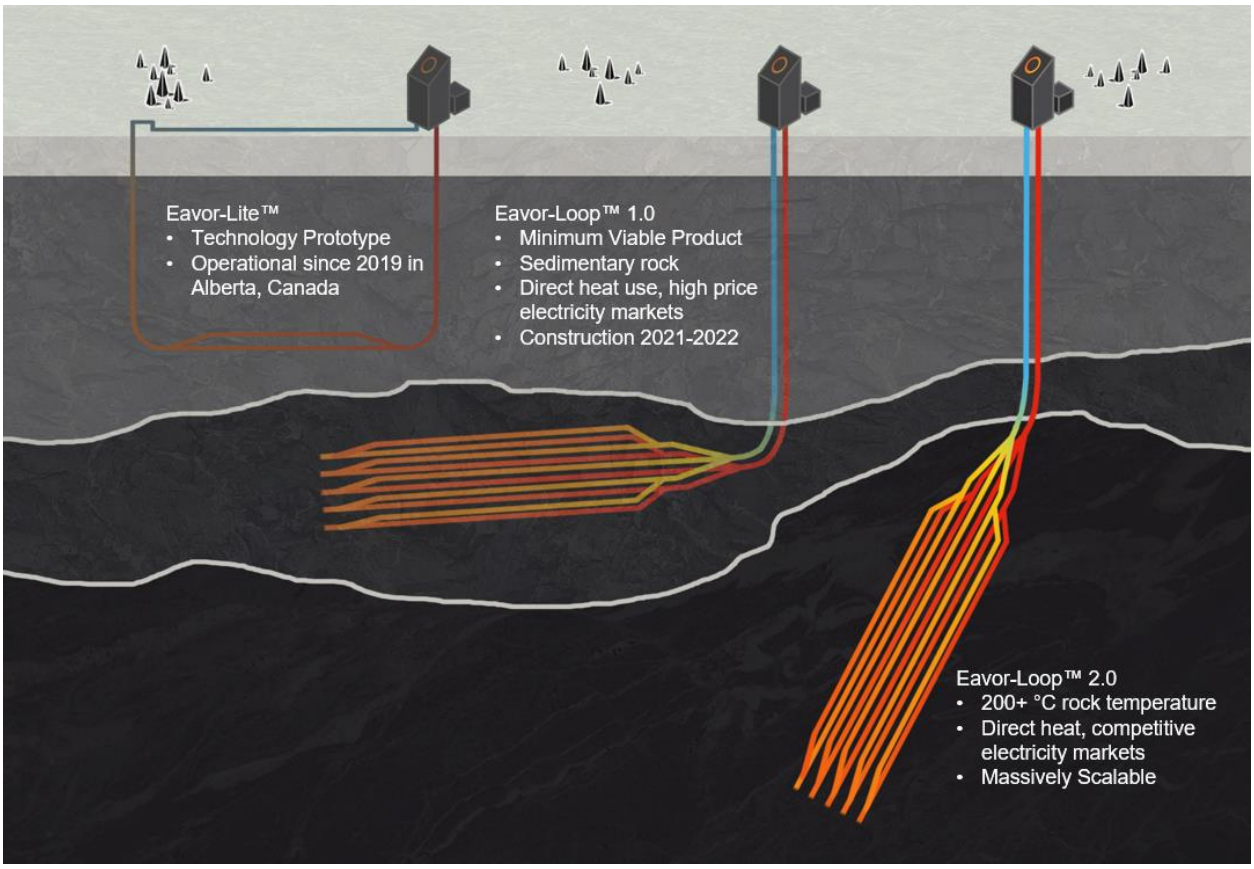

Figure 8: Eavor-Loop™ evolution

This paper considers a case study for a futuristic project drilled in a high geothermal gradient environment, where the Eavor-Loop™ is drilled into rock with an average temperature exceeding 200°C. While drilling such a project is not possible with today's technology, Eavor has been progressing numerous research and development initiatives to make such a project a reality. The details of these initiatives are both proprietary and outside the scope of this paper, but Eavor has line of sight to LCOE below US$50/MWh with technology anticipated to be proven in 2022.

The proposed deep Eavor-Loop™ was modelled utilizing Eavor's transient model. Net heat to power efficiency was calculated based on the outlet wellhead temperature, an assumed utilization efficiency of 50% (relative to Carnot efficiency), and an assumed cold sink temperature of 15°C:

$$\eta = 0.5\left(1 - \frac{15+273.15}{T_H+273.15}\right) \quad (7)$$

where η is net heat to power efficiency
T_H is the produced fluid temperature at the outlet wellhead

The simulated electrical power for operation with a constant flowrate is shown in Figure 9. Alternatively, the loop can be operated with a variable flowrate to give a constant power output suitable for baseload operation, shown in Figure 10. Both simulations were run for a period of 20 years.

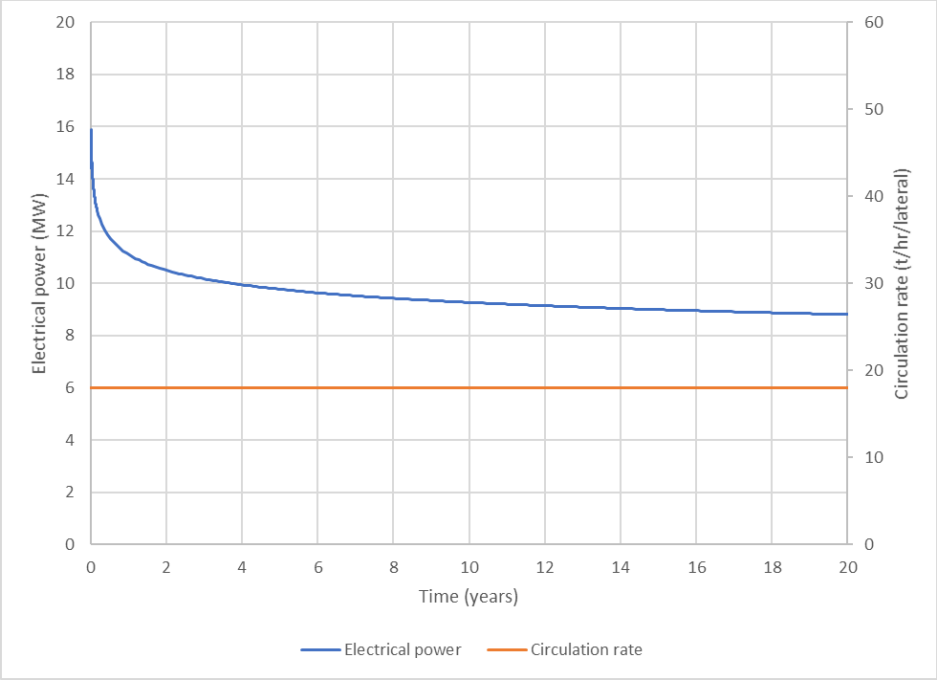

Figure 9: Simulated electrical power for the deep Eavor-Loop™ 2.0 under constant flowrate operation

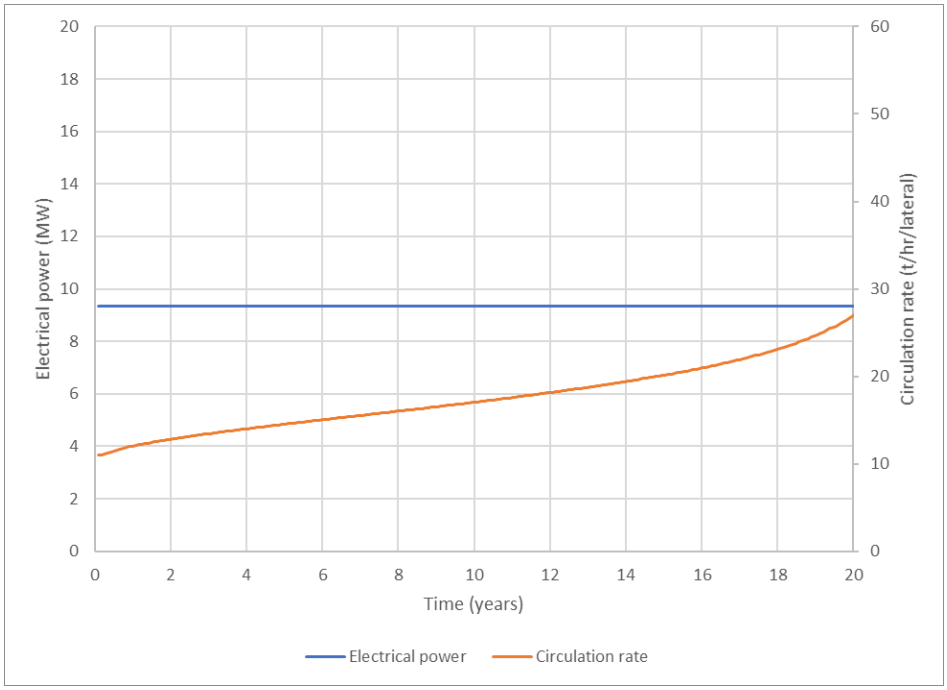

Figure 10: Simulated electrical power for the deep Eavor-Loop™ 2.0 under baseload operation

As validated by the thermal recharge tests at Eavor-Lite™, the transient model can predict the thermal response of the rock matrix to changes in circulation rate. This capability can be used to demonstrate the ability of the Eavor-Loop™ to operate in a flexible fashion, storing energy by ramping down (or shutting in) during periods of low demand and then increasing the flowrate and producing that energy during periods of high demand. The rock, coupled with the large subsurface volume of the loop itself, acts as a battery, controlled by manipulating the flowrate. To produce the excess power on demand, no design changes to the loop are required but the surface heat to power capacity must be increased. The key parameters for modelling flexible operation are the dispatch ratio d, defined as the maximum power output of the system divided by the rated (baseload) capacity; and the recharge ratio r, defined as the power output during the recharge phase divided by the rated (baseload) capacity. For lossless diurnal flexibility, the cumulative generation (MWh) at the end of the day remains constant for all values of d and r. Enforcing this daily energy balance gives the following equation for how many hours per day the loop can operate at its peak power output:

$$t_d = \frac{24(1-r)}{d-r} \tag{8}$$

And accordingly:

$$t_r = 24 - t_d \tag{9}$$

In this section, two cases are presented:

1. Dispatch ratio = 1.5, recharge ratio = 0.3 (low ratio flexibility)
2. Dispatch ratio = 2.0, recharge ratio = 0.0 (high ratio flexibility)

Both cases were modelled for 20 years of diurnal cycles. A snapshot of the transient behaviour of cases 1 and 2 are shown in Figure 11 and Figure 12, respectively. Cumulative power generation at

the end of 20 years for all four cases are compared in Table 1. These results prove the ability of the Eavor-Loop™ to store energy and operate in a flexible manner over a multi-decade period.

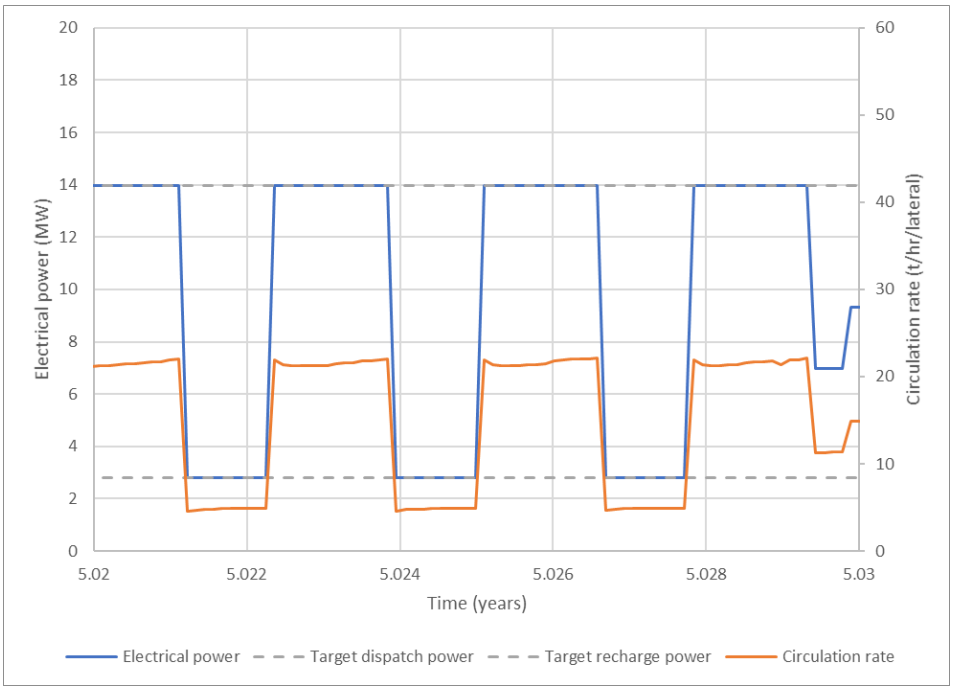

Figure 11: Load-matching power output and circulation rate profile for 3 representative days of case 1 (dispatch ratio = 1.5, recharge ratio = 0.3)

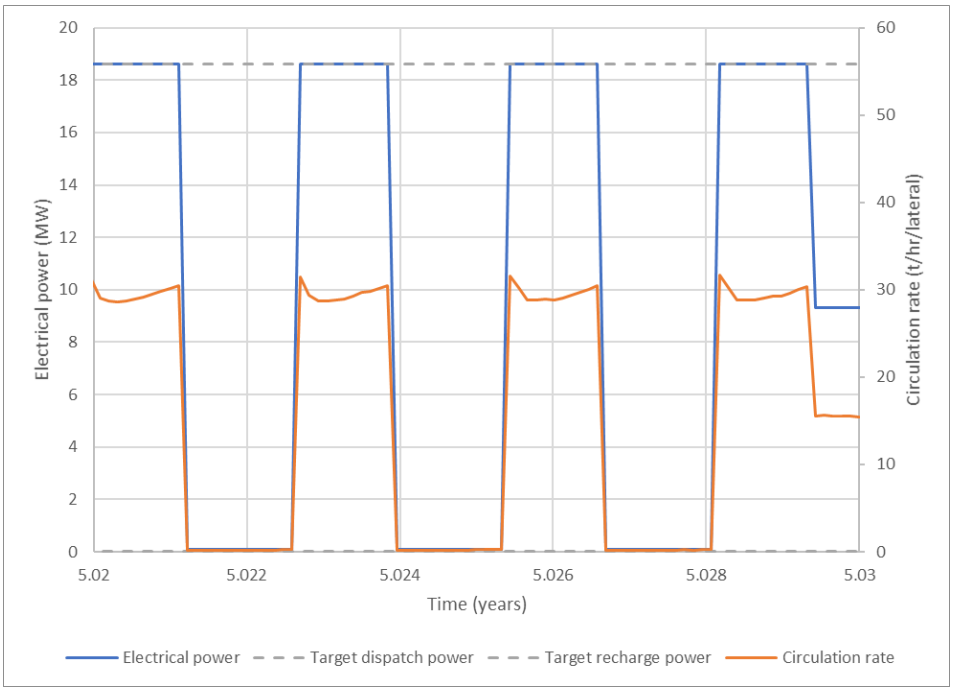

Figure 12: Load-matching power output and circulation rate profile for 3 representative days of case 2 (dispatch ratio = 2.0, recharge ratio = 0.0)

Table 1: Cumulative power generation after 20 years of simulation for various Eavor-Loop™ operating modes

	Cumulative power generation in 20 years (GWh)	Average power generation (MW)	Change relative to constant flowrate case
Constant flowrate	1,669	9.53	
Baseload	1,640	9.36	-1.8%
Flexible (low ratio)	1,665	9.51	-0.2%
Flexible (high ratio)	1,552	8.86	-7.0%

3. Electrical grid modelling

3.1 Model overview

To demonstrate the value of Eavor-Loop™ in achieving a net-zero electricity grid, an electricity resource capacity expansion model (GenX) was used. GenX is a constrained optimization model that determines the mix of electricity generation and storage required to meet electricity demand while minimizing total system cost (Jenkins & Sepulveda, 2017). A case study of the United States Western Interconnection grid was analyzed in a net-zero 2050 scenario.

The Western Interconnect grid was divided into six zones (Figure 13). Each zone is treated as a node and capacity constraints are defined on inter-zone electricity transmission. Within each zone, electricity demand and resource availability are modelled at hourly intervals, with 3,360 representative hours (20 weeks) used to model a single year. The GenX model determines the optimal mix of resources and their operation to match supply and demand at each hour while minimizing total system cost.

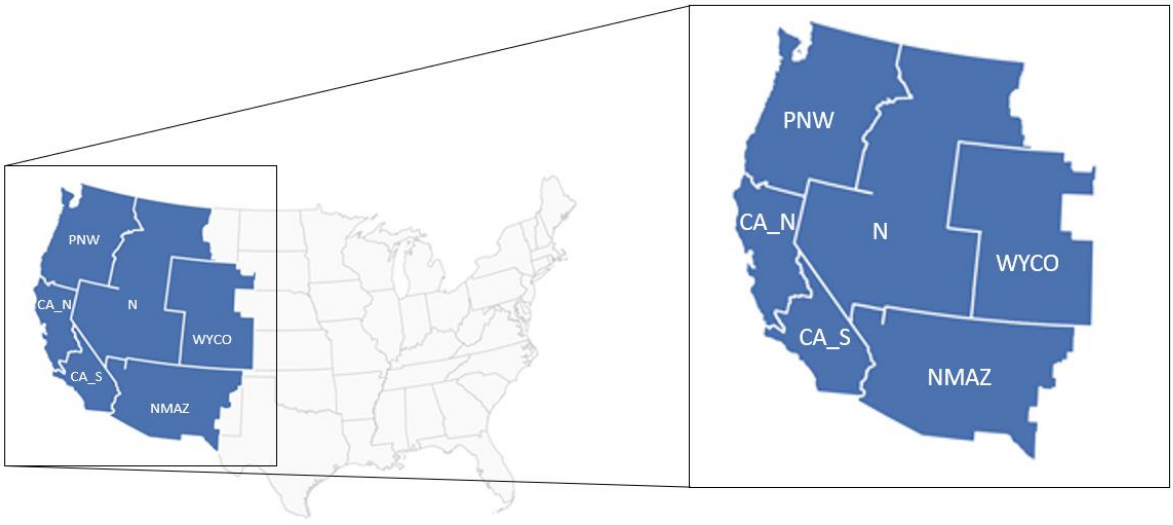

Figure 13: Western Interconnect grid zonal divisions for GenX model

The optimal resource mix is heavily dependent on total electricity demand as well as cost and availability of competing resource types. Two competing technology cost scenarios, summarized

in Table 2, and two demand scenarios, summarized in Table 3, were defined. All costs are in USD and are on a per kilowatt basis, unless otherwise specified.

Table 2: Competing technology cost assumptions

	Low cost	High cost	Reference
Wind	$761	$1,121	(1)
Solar	$516	$669	(1)
Battery (capacity)	$73	$121	(1)
Battery (energy) ($/kWh)	$84	$139	(1)
Nuclear	$4,650	n/a	(1)
New natural gas combined cycle (NGCC) + carbon capture and storage (CCS)	$1,599	$3,198	(1)
Retrofit NGCC with CCS	$1,279	n/a	(1)
Retrofit combined cycle (CC) for zero-carbon fuels	$419	$419	(1)
Retrofit combustion turbine (CT) for zero-carbon fuels	$333	$333	(1)
New CC for zero-carbon fuels	$856	$856	(1)
New CT for zero-carbon fuels	$667	$667	(1)
Zero-carbon fuel ($/MMBTU)	$9	$18	(2)
Equivalent cost assuming hydrogen ($/kg)	*$1.20*	*$2.43*	(2)
Natural gas (Pacific) ($/MMBTU)	$3.61	$7.27	(3)
Natural gas (Mountain) ($/MMBTU)	$3.73	$7.77	(3)

(1) (National Renewable Energy Laboratory, 2020)
(2) (Larson et al., 2020)

Table 3: Electricity demand assumptions

	Moderate demand	High demand	Reference
Annual demand (TWh)	1,410	1,685	(3)
Flexible EV capacity (MW)	81,974	134,726	(2)
Flexible heat pump capacity (MW)	27,239	31,480	(2)
Flexible water heat capacity (MW)	5,526	5,988	(2)

(3) (U.S. Energy Information Administration, 2020)

In addition, the following assumptions were made on the ability to retrofit existing infrastructure:

- Capacity for retrofitting NGCC with CCS limited to 50% of existing NGCC capacity
- Capacity for retrofitting CC for zero-carbon fuels limited to 50% of existing CC capacity when CCS upgrades available, 100% when CCS not available

3.2 Model incorporation of Eavor-Loop™

Each of the 6 zones were discretized into candidate project areas (CPAs) on the order of 10 km^2 per CPA. Within each CPA, geothermal gradient was mapped using Curie point data (Li, Lu, & Wang, 2017). Exclusion zones were applied for non-developable areas, such as water bodies, mountain ranges, national parks, military land, and proximity to critical infrastructure. Two transmission costs were calculated for each CPA, with the lower of the two used by the model. The first cost assumes construction of a new spur line directly from the CPA to a load center. The second cost assumes construction of a new spur line to an existing high-voltage line and transmission on the high-voltage line to a load center.

Curves were generated for Eavor-Loop™ power output as a function of geothermal gradient using the thermodynamic model and assuming operation in baseload mode. Capital and operating costs were calculated based on Eavor's proprietary technology roadmap and internal cost assumptions. For each CPA, a generation potential was calculated using the Eavor-Loop™ footprint, area of the CPA, and power generated from a single Eavor-Loop™ based on the CPA's geothermal gradient. Each CPA was also assigned an LCOE inclusive of transmission using the cost assumptions already discussed. The CPAs within each region were aggregated and ranked to produce the regional Eavor-Loop™ supply curves shown in Figure 14.

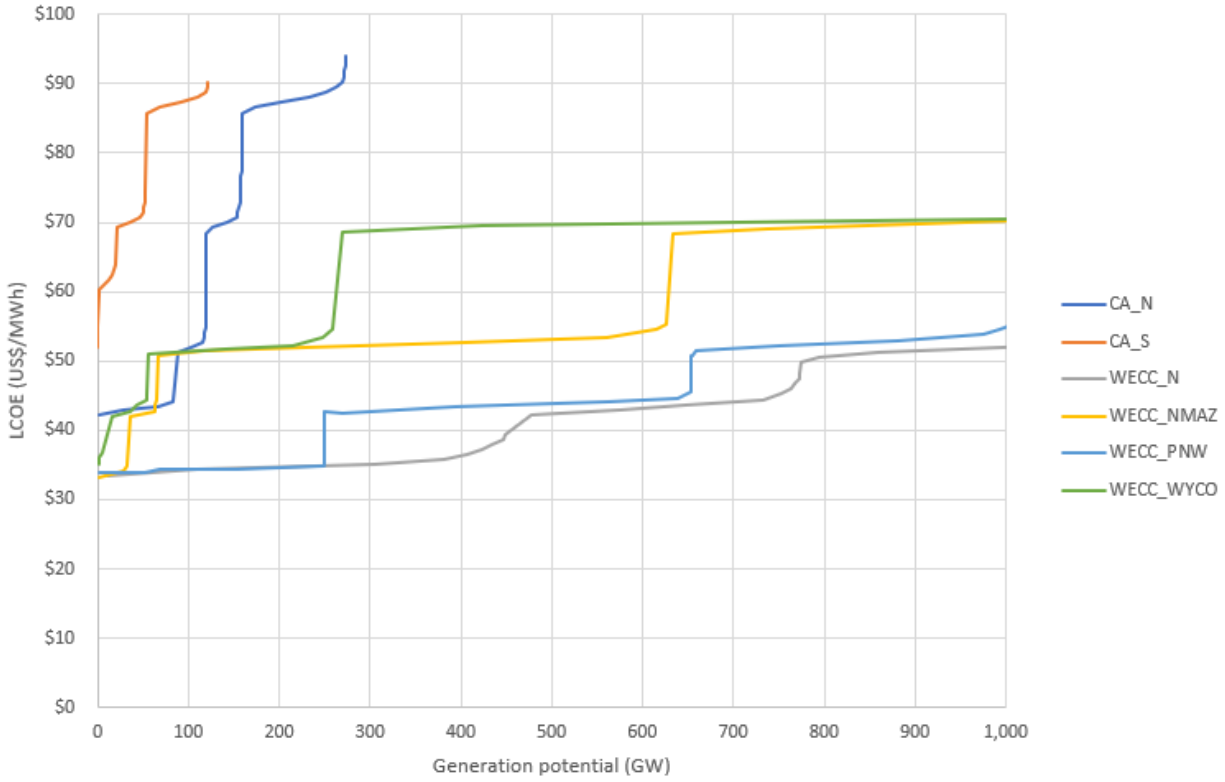

Figure 14: Eavor-Loop™ regional supply curves used as inputs to the GenX model

To model flexible operation, costs were further divided into a capacity (surface) component and a charge (subsurface) component. The total Eavor-Loop™ investment cost is the sum of the capacity and charge components. GenX was modified to optimize investments in surface and subsurface capacity independently to deliver the lowest total system cost. For example, if the model chooses

to build 1 GW of subsurface capacity with a dispatch ratio of 1.5, it would build 1.5 GW of surface capacity. At any point in time, the system can deliver up to 1.5 GW of power but is constrained to an average power output over the representative week of 1 GW (or a total generation of 168 GWh per week). The energy "charge" from the subsurface is assumed to be constant, and the discharge rate is governed by the surface capacity and the optimal system dispatch to supply demand at minimum cost.

All cases are compared based on the total system cost, mainly comprised of annuitized capital investment and any fixed or variable operating and maintenance costs. All scenarios were run with and without Eavor-Loop™ as an option to quantify the technology value as the total system cost savings when Eavor-Loop™ is available. For Eavor-Loop™ scenarios, key outputs are the capacity built, total energy produced, and hourly dispatch patterns.

3.3 Model results

This paper will focus on the two extreme cases for Eavor-Loop™ adoption: high demand and high-cost alternative generation technologies (most optimistic case for Eavor-Loop™); and moderate demand and low-cost alternative generation technologies (most pessimistic case for Eavor-Loop™).

3.3.1 Optimistic case: high demand and high-cost alternative generation

In the high demand and high-cost alternative generation scenario, the total annual system costs with and without Eavor-Loop™ are $75.4B and $95.6B, respectively. Inclusion of Eavor-Loop™ in the capacity optimization results in annual system cost savings of over $20B (a 21% reduction). Without Eavor-Loop™, generation is provided primarily by solar and wind (Figure 15). Over 50% of total system cost is allocated to providing firmness and reliability, split primarily amongst gas + CCS, zero carbon fuel, batteries, and other renewables (hydrothermal) (Figure 16). When the model has the option to build Eavor-Loop™, it supplies 40% of the total electricity generation. The $32B annual cost of the Eavor-Loops™ is more than offset by $35B in reduced spending on the aforementioned firmness and reliability-providing technologies. The remainder of the cost savings are realized through reduced investments in wind and solar.

Building 90 GW of Eavor-Loop™ capacity eliminates the need for 200 GW of other capacity, reducing total capacity required to meet demand by 110 GW (Figure 17). This reduction includes 35 GW of reduced solar and 91 GW of reduced wind capacity. Any type of capacity requires land use, and both solar and wind have large footprints, with median energy generation densities of 6.63 and 1.84 W/m^2 for solar and wind power, respectively (van Zalk & Behrens, 2018). Internal calculations give the energy generation density of Eavor-Loop™ at 363 W/m^2. In this case, inclusion of Eavor-Loop™ reduces total land requirement for solar and wind by approximately 9,000 km^2 (2.2 million acres or 43%), equivalent to land savings of 25 acres/MW of Eavor-Loop™ capacity.

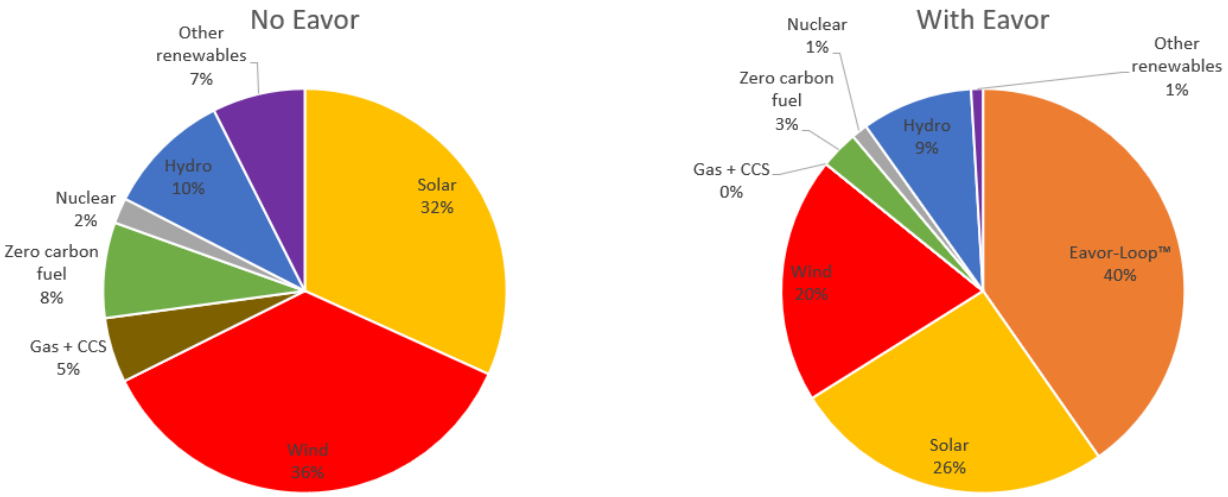

Figure 15: Energy share profiles without Eavor-Loop™ (left) and with Eavor-Loop™ (right) for the high demand and high-cost alternative generation scenario

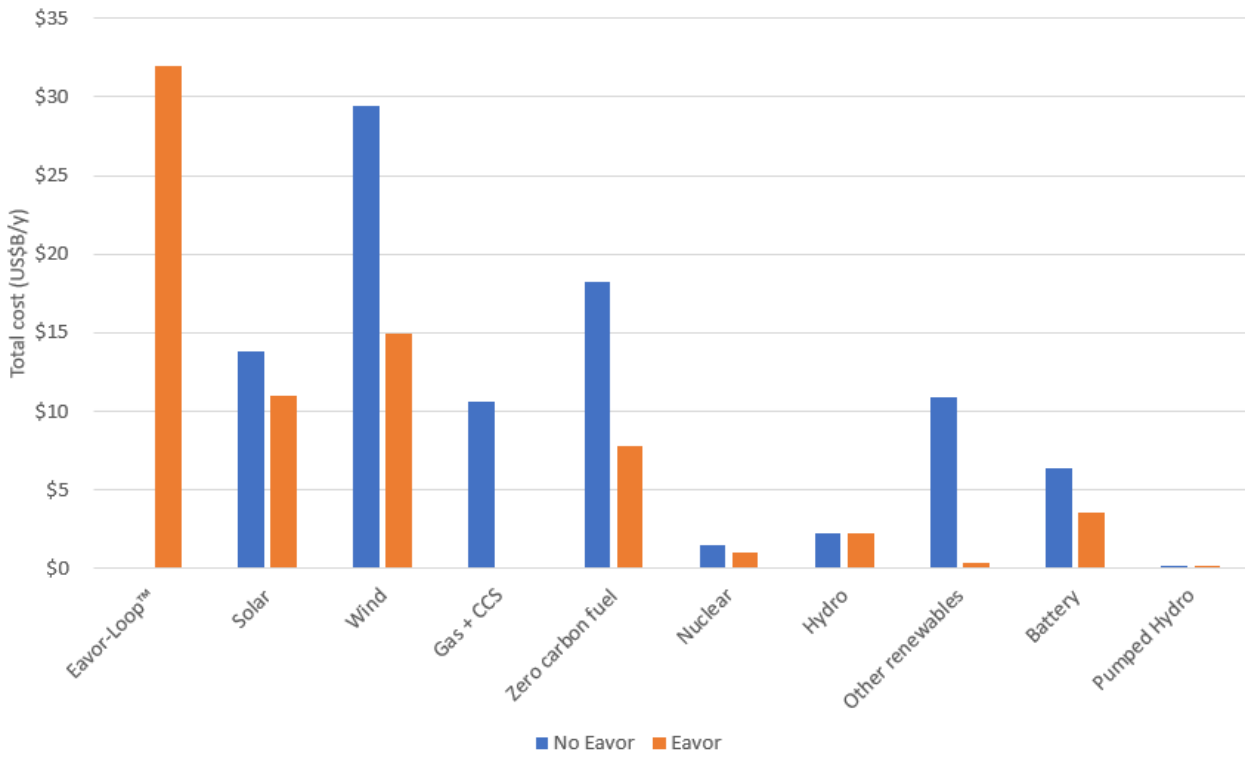

Figure 16: Components of total system cost with and without Eavor-Loop™ for the high demand and high-cost alternative generation scenario

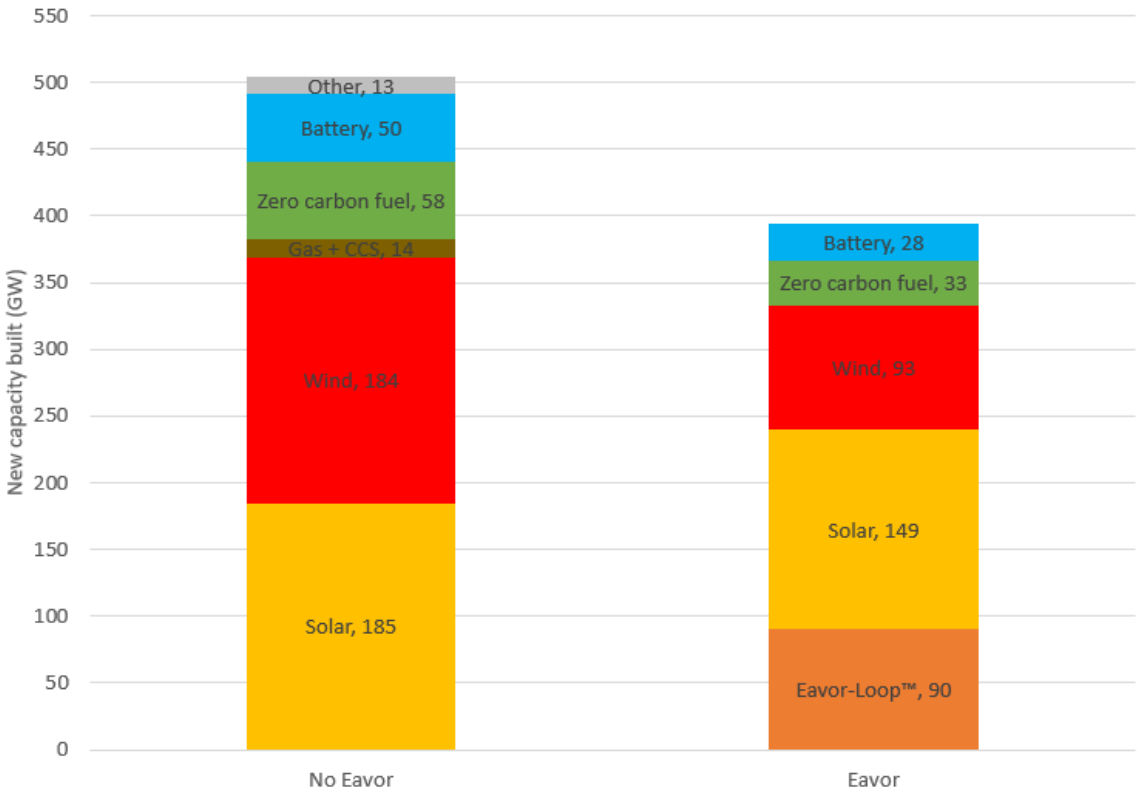

Figure 17: Breakdown of new capacity built with and without Eavor-Loop™ for the high demand and high-cost alternative generation scenario

3.3.2 Pessimistic case: moderate demand and low-cost alternative generation

In the moderate demand and low-cost alternative generation scenario, the total annual system costs with and without Eavor-Loop™ are $50.0B and $52.2B, respectively. Even in this worst-case scenario for Eavor-Loop™ value, its inclusion results in annual savings of over $2B and it provides 19% of the total electricity generation (Figure 18). All trends observed in the previous scenario remain, albeit with a reduced magnitude given the lower overall system cost and the smaller, but still significant, penetration of Eavor-Loop™ into the grid. Generation without Eavor-Loop™ is still provided primarily by solar and wind. Over 50% of total system cost is once again allocated to providing firmness and reliability, and the annual cost of Eavor-Loop™ ($10B) is nearly entirely offset by reduced spending for such technologies ($8B) (Figure 19). The remainder of the cost savings come from reduced spending on solar and wind. Again, inclusion of Eavor-Loop™ reduces total capacity required to meet demand. In this case, capacity is reduced by 43 GW (including 22 GW reduced solar and 26 GW reduced wind), land usage due to solar and wind is reduced by 2,800 km^2 (700 thousand acres or 20%), and land savings are 22 acres/MW of Eavor-Loop™ capacity.

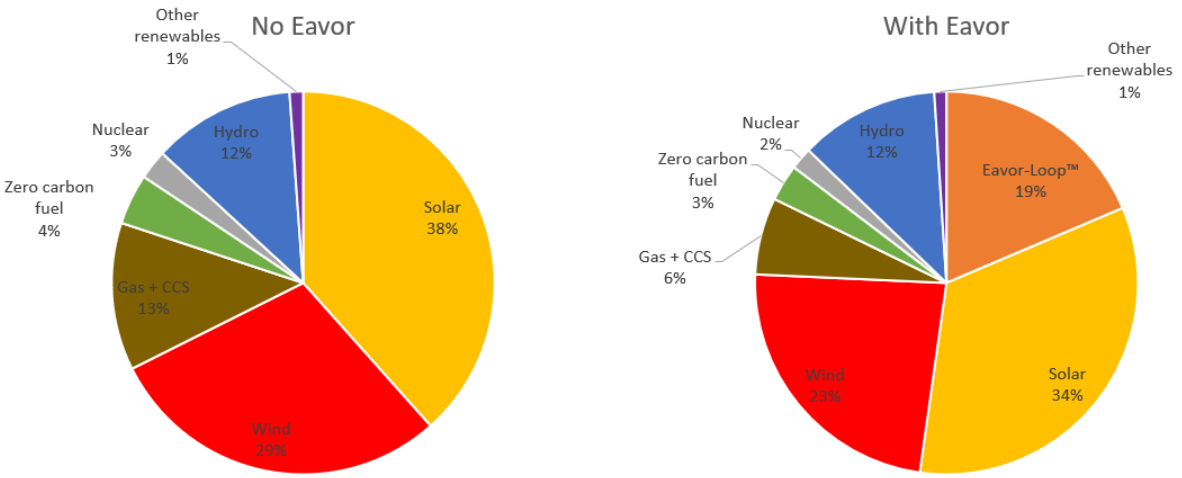

Figure 18: Energy share profiles without Eavor-Loop™ (left) and with Eavor-Loop™ (right) for the moderate demand and low-cost alternative generation scenario

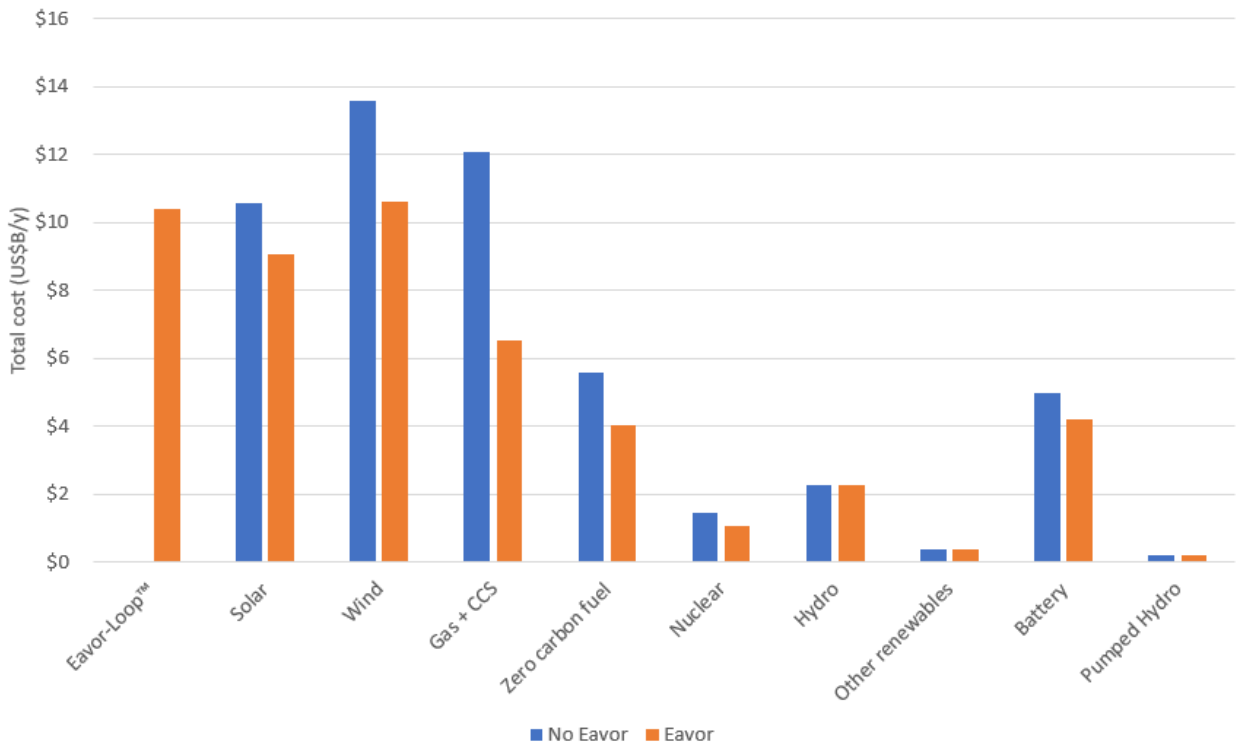

Figure 19: Components of total system cost with and without Eavor-Loop™ for the moderate demand and low-cost alternative generation scenario

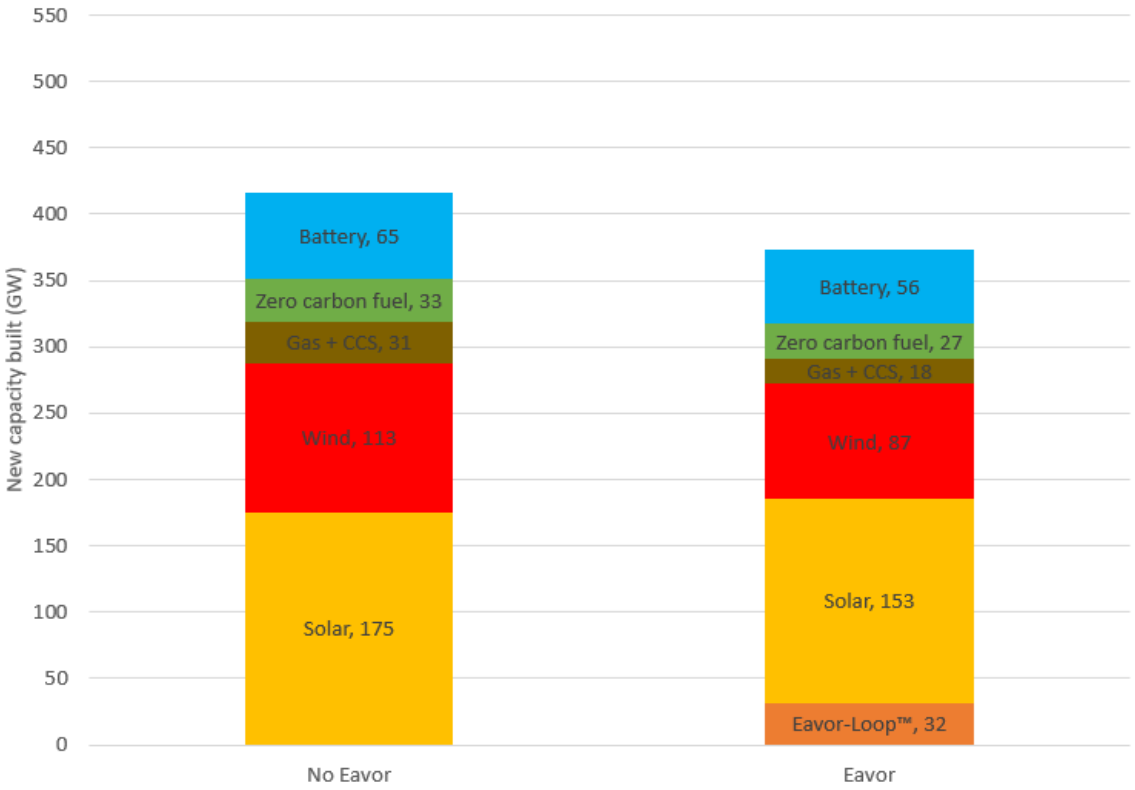

Figure 20: Breakdown of new capacity built with and without Eavor-Loop™ for the moderate demand and low-cost alternative generation scenario

3.3.3 Additional sensitivities

In the absence of Eavor-Loop™, GenX relies heavily on other zero-emission firm capacity, primarily gas + CCS and zero carbon fuels. Neither of these technologies are currently at a commercially viable stage and are by no means guaranteed to be available in the future, let alone at the prices assumed in the model. To understand the impact of this assumption, additional sensitivities were run in which no zero-emission firm capacity options were available (except for Eavor-Loop™ as applicable). In these scenarios, all future demand must be met by a combination of wind and solar, with batteries available to time-shift the output as necessary to meet demand.

In the high demand and high-cost alternative generation scenario, total annual system cost with and without Eavor-Loop™ was $96.8 and $499.7B, respectively. Without zero-emission firm resources, the total system cost for the no Eavor-Loop™ scenario increased 5-fold (from $95.6B to $499.7B) while the scenario with Eavor-Loop™ increased by only 28% (from $75.4B to $96.8B). The substantial cost savings come from reduced spending on wind and batteries as well as a significant penalty associated with demand curtailment (Figure 21). The demand curtailment, or value of lost load, refers to the social cost of not serving demand. It means the model could not provide supply to match demand at a cost below $9,000/MWh, triggering unserved demand. In real life, this indicates a grid reliability issue and would translate to forced curtailment or rolling blackouts.

In the moderate demand and low-cost alternative generation scenario, total annual system cost with and without Eavor-Loop™ was $57.0B and $106.4B, respectively. In this case, the absence of zero-emission firm resources doubled the no Eavor-Loop™ scenario costs (from $52.2B to $106.4B), while the scenario with Eavor-Loop™ saw only a modest cost increase of 14% (from $50.0B to $57.0B). In this scenario, there was no substantial demand curtailment and cost savings are realized primarily through reduced spending on wind and batteries (Figure 22).

In addition to the cost savings, both scenarios give substantial land savings, summarized below.

Table 4: Key land use reduction metrics for the sensitivity cases

	High demand, high-cost alternative generation	Moderate demand, low-cost alternative generation
Reduction in land usage (km^2)	13,600	11,500
Reduction in land usage (acres)	3.4 million	2.8 million
Reduction in land usage (%)	49%	45%
Land savings (acres/MW Eavor-Loop™ capacity)	48	36

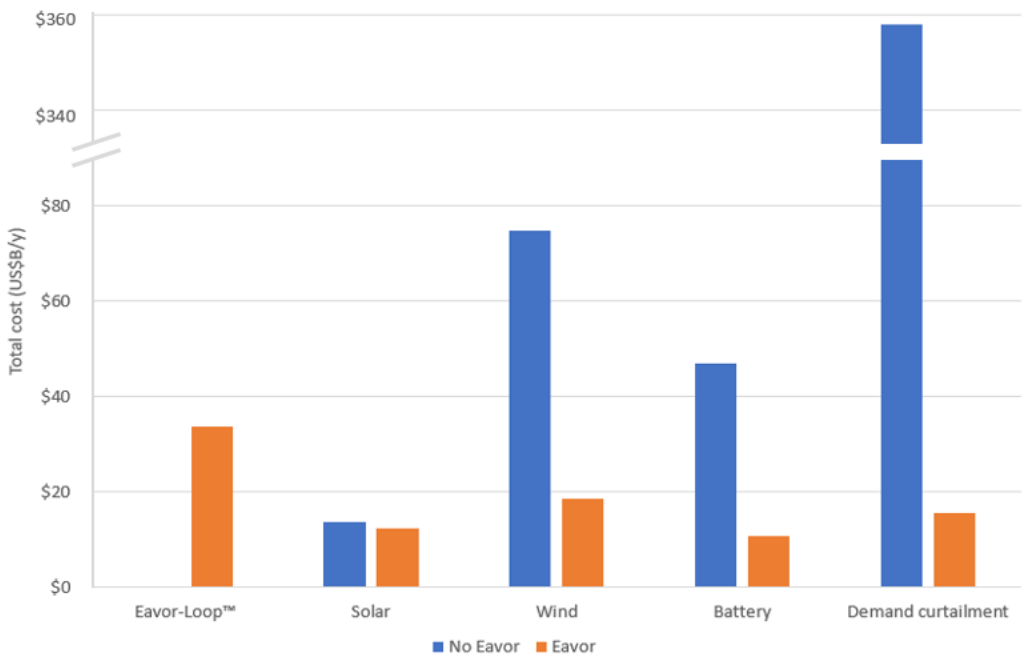

Figure 21: Components of total system cost with and without Eavor-Loop™ for the scenario with high demand, high-cost alternative generation, and no firm capacity (other than Eavor-Loop™). Note the discontinuous y-axis.

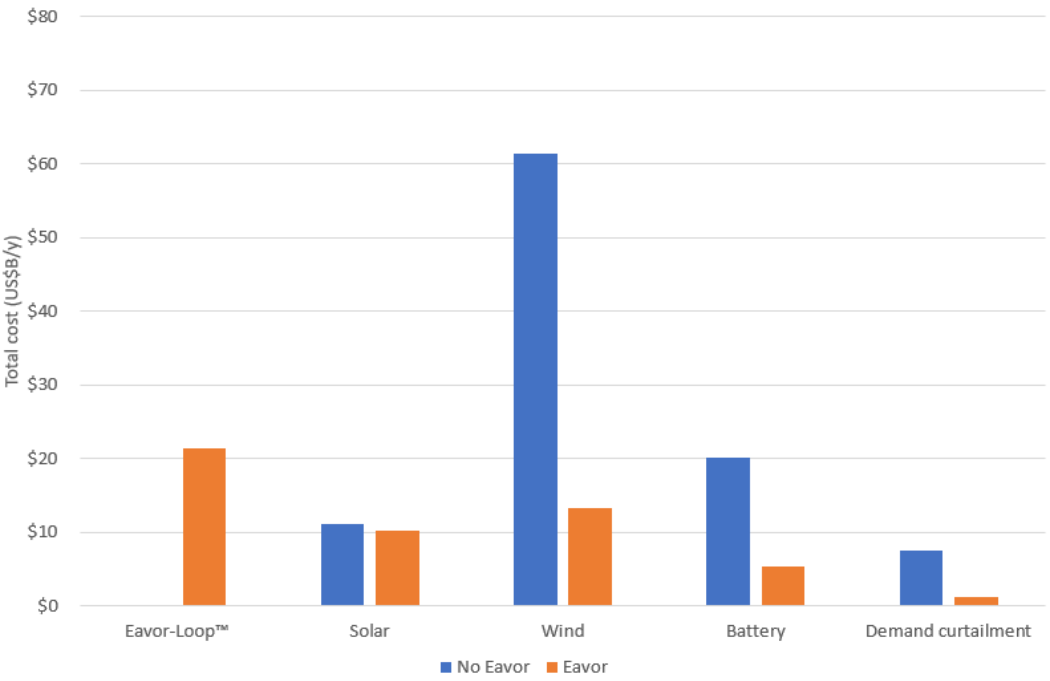

Figure 22: Components of total system cost with and without Eavor-Loop™ for the scenario with moderate demand, low-cost alternative generation, and no firm capacity (other than Eavor-Loop™)

3.3.4. Flexible operation

As discussed in section 3.2, GenX was modified to optimize investments in surface and subsurface capacity independently to deliver the lowest total system cost. Model results give optimized Eavor-Loop™ dispatch ratios ranging from 1.00 (baseload operation) to 1.81, depending in part on the contribution of solar and wind to the zone's overall electricity generation (Figure 23). These dispatch ratios are well within the range modelled and proven to be feasible in section 2.5, thus confirming the ability of the Eavor-Loop™ to operate as a zero-emissions load-following resource in an economically optimized fashion.

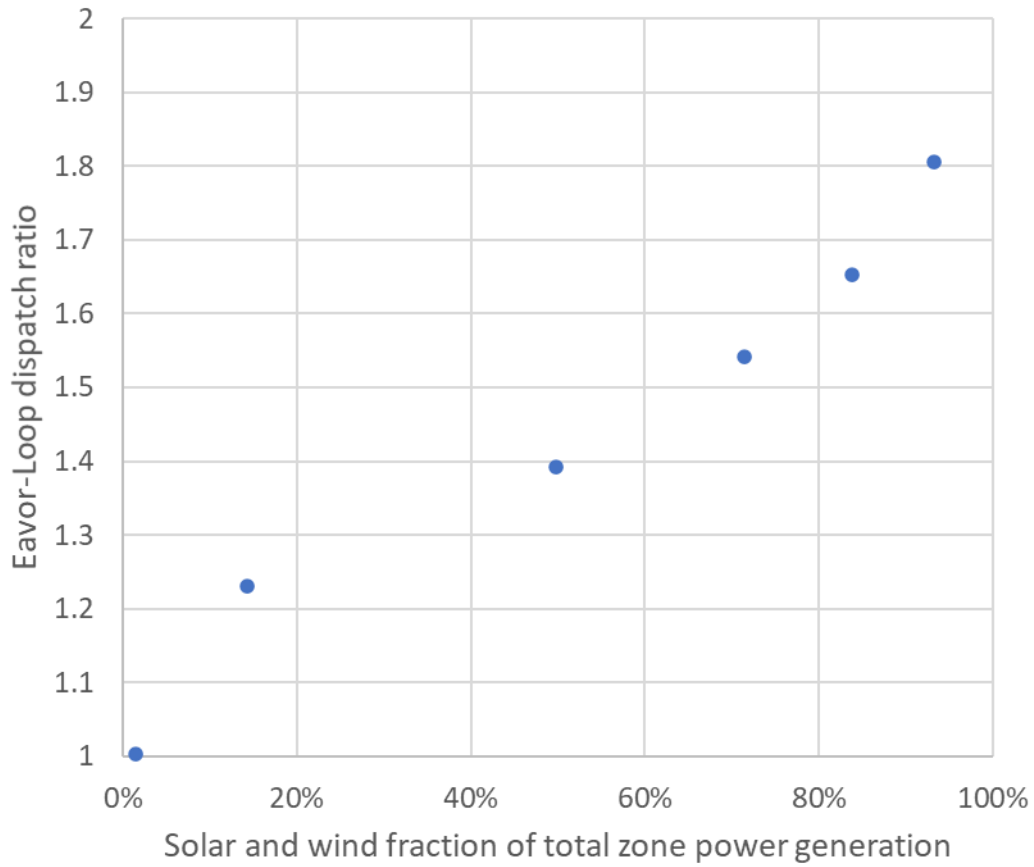

Figure 23: Optimized Eavor-Loop™ dispatch ratio as a function of grid dependency on intermittent renewable generation

Analysis of the dispatch patterns revealed diurnal cycling of the Eavor-Loops™ inversely correlated with solar output. Two representative dispatch patterns are shown below. Figure 24 shows one representative week from the Southern California zone, powered 56% by solar and 15% by wind. A dispatch ratio of 1.54 and recharge ratio of 0 are observed. Figure 25 shows one representative week from the Northern California zone, powered only 14% by solar with no wind. Here, a dispatch ratio of 1.23 is observed, with recharge ratio ranging from 0 to 0.69.

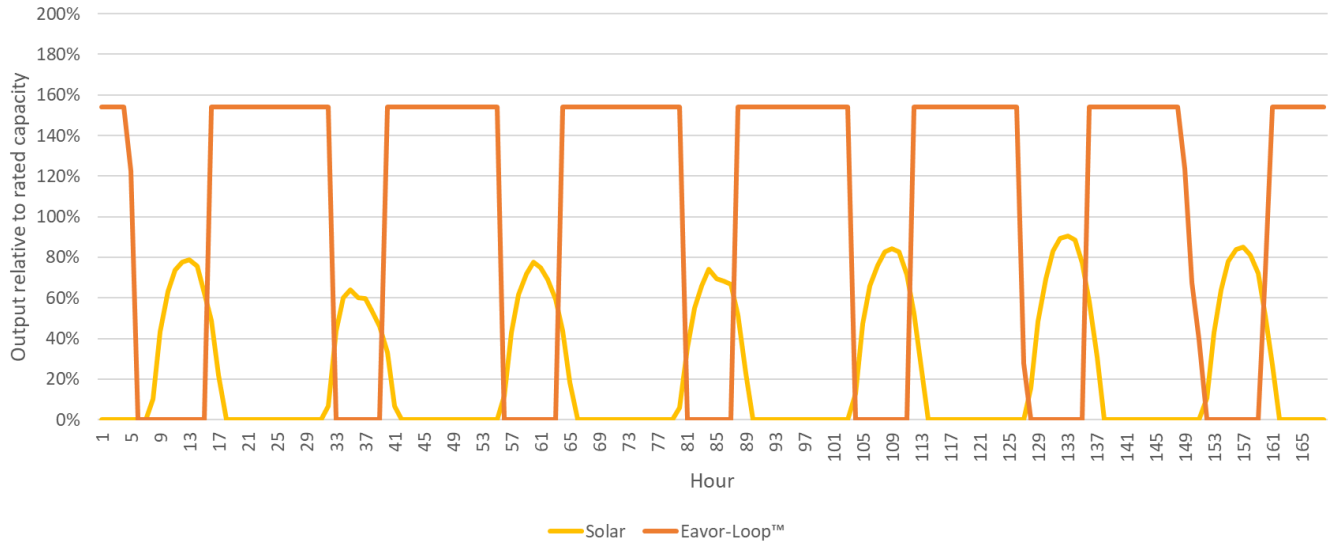

Figure 24: Dispatch pattern of Eavor-Loop™ and solar in one representative week in the Southern California zone

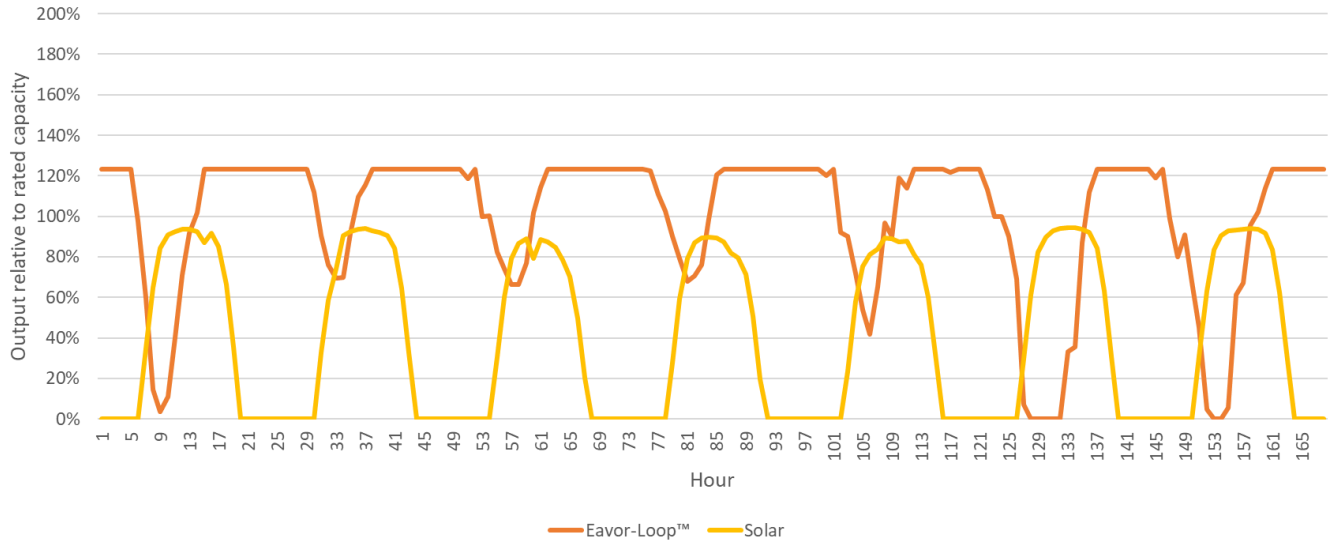

Figure 25: Dispatch pattern of Eavor-Loop™ and solar in one representative week in the Northern California zone

4. Conclusion

The Eavor-Loop™ was introduced as a multilateral closed-loop geothermal system that is globally scalable and capable of providing grid stability and resiliency. A transient, fully coupled wellbore + thermal model was developed and validated using over 16 months of operational data from an Eavor-Loop™ field demonstration project in Alberta, Canada. Recent modelling work, coupled with field trials, has proven the feasibility of the Eavor-Loop™ to provide flexible energy generation for load-balancing or peak-matching with a minimal impact on lifetime energy extraction. Transient operation allows the system to recharge during low demand periods and discharge this stored energy during high demand periods.

The value of the Eavor-Loop™ in a net-zero grid was modelled with a case study of the United States Western Interconnection power transmission grid using an electricity resource capacity expansion model (GenX). The modelling indicates that the Eavor-Loop™ can reduce the annual total system cost by up to $20B (21%) in a base case and up to $403B (81%) in an extreme case. These cost savings are achieved through:

1. Reduced spending on other technologies providing firmness and reliability such as gas + CCS, zero carbon fuel (i.e., hydrogen), and batteries
2. Reduced spending on intermittent renewables, namely solar and wind

Inclusion of the Eavor-Loop™ enables 100% renewable energy power systems while reducing required installed capacity of land-heavy resources such as solar and wind by up to 49%, saving 22 acres in the base case and up to 48 acres in the extreme case for each megawatt of Eavor-Loop™ installed. The Eavor-Loops™ are operated in a diurnal pattern inversely correlated to solar power generation. The system is allowed to recharge while the sun is shining and then dispatches the stored energy when the sun goes down. Optimized dispatch patterns from the GenX model were validated with the transient thermodynamic model, proving both the technical feasibility and value potential of the Eavor-Loop™ technology.

REFERENCES

bp. (2020). *Statistical review of world energy*.

European Commission. (2020). *Powering a climate-neutral economy: An EU Strategy for Energy System Integration.* Brussels.

Fallah, A., Gu, Q., Chen, D., Ashok, P., van Oort, E., & Holmes, M. (2021). Globally scalable geothermal energy production through managed pressure operation control of deep closed-loop well systems. *Energy Conversion and Management*.

Horne, R. (1980). Design considerations of a down-hole coaxial geothermal heat exchanger. *Geothermal Resources Council Transactions*.

International Energy Agency. (2021). *Net zero by 2050: A roadmap for the global energy sector.*

Jenkins, J. D., & Sepulveda, N. A. (2017). *Enhanced decision support for a changing electricity landscape.* Cambridge, MA: MIT Energy Initiative.

Kutun, K., Tureyen, O., & Satman, A. (2015). Analysis of wellhead production temperature derivatives. *Fortieth workshop on geothermal reservoir engineering.* Stanford, CA: Stanford University.

Larson et al. (2020). *Net-Zero America: Potential Pathways, Infrastructure, and Impacts.* Princeton University.

Li, C.-F., Lu, Y., & Wang, J. (2017). A global reference model of Curie-point depths based on EMAG2. *Scientific Reports*.

Morita, K., Tago, M., & Ehara, S. (2005). Case study on small-scale power generation with downhole coaxial heat exchanger. *World Geothermal Congress.* Atalya, Turkey.

Nalla, G., Shook, G., Mines, G., & Bloomfield, K. (2005). Parametric sensitivity study of operating and design variables in wellbore heat exchangers. *Geothermics*.

National Institute of Standards and Technology. (2020). REFPROP.

National Renewable Energy Laboratory. (2018). *Electrification futures study: scenarios of electric technology adoption and power consumption for the United States.* Golden, CO.

National Renewable Energy Laboratory. (2020). Annual Technology Baseline.

Oldenberg, C., Pan, L., Muir, M., Eastman, A., & Higgins, B. (2016). Numerical simulation of critical factors controlling heat extraction from geothermal systems using a closed-loop heat exchange method. *41st workshop on geothermal reservoir engineering.* Stanford, CA: Stanford University.

Ramey Jr, H. (1962). Wellbore heat transmission. *Journal of Petroleum Technology*, 427-435.

Rybach, L. (2010). The future of geothermal energy and its challenges. *World Geothermal Congress.*

Sepulveda, N. A., Jenkins, J. D., de Sisternes, F. J., & Lester, R. K. (2018). The role of firm low-carbon electricity resources in deep decarbonization of power generation. *Joule*.

Toews, M., Riddell, D., Vany, J., & Schwarz, B. (2020). Case study of a multilateral closed-loop geothermal system. *World Geothermal Congress.* Reykjavik.

U.S. Energy Information Administration. (2020). Annual Energy Outlook.

van Zalk, J., & Behrens, P. (2018). The spatial extent of renewable and non-renewable power generation: A review and meta-analysis of power densities and their application in the U.S. *Energy Policy*.